PHOTONICS Research

Tunable and switchable harmonic h-shaped pulse generation in a 3.03 km ultralong mode-locked thulium-doped fiber laser

Junqing Zhao,[1] Lei Li,[1] Luming Zhao,[1,2,*] Dingyuan Tang,[1] Deyuan Shen,[1] and Lei Su[2]

[1]Jiangsu Key Laboratory of Advanced Laser Materials and Devices, Jiangsu Collaborative Innovation Center of Advanced Laser Technology and Emerging Industry, School of Physics and Electronic Engineering, Jiangsu Normal University, Xuzhou 221116, China
[2]School of Engineering and Materials Science, Queen Mary University of London, London, UK
*Corresponding author: lmzhao@ieee.org

Received 31 October 2018; revised 20 January 2019; accepted 23 January 2019; posted 24 January 2019 (Doc. ID 349711); published 27 February 2019

We experimentally demonstrated a type of tunable and switchable harmonic h-shaped pulse generation in a thulium-doped fiber (TDF) laser passively mode locked by using an ultralong nonlinear optical loop mirror. The total cavity length was ~3.03 km, the longest ever built for a TDF laser to our best knowledge, which resulted in an ultralarge anomalous dispersion over −200 ps^2 around the emission wavelength. The produced h-shaped pulse can operate either in a fundamental or in a high-order harmonic mode-locking (HML) state depending on pump power and intra-cavity polarization state (PS). The pulse duration, no matter of the operation state, was tunable with pump power. However, pulse breaking and self-organizing occurred, resulting in high-order HML, when the pump power increased above a threshold. At a fixed pump power, the order of HML was switchable from one to another by manipulating the PS. Switching from the 8th up to the 48th order of HML was achieved with a fixed pump power of ~4.15 W. Our results revealed the detailed evolution and switching characteristics of the HML and individual pulse envelope with respect to both the pump power and PS. We have also discussed in detail the mechanisms of both the h-shaped pulse generation and the switching of its HML. This contribution would be helpful for further in-depth study on the underlying dynamics of long-duration particular-envelope pulses with ultralarge anomalous dispersion and ultralong roundtrip time.

https://doi.org/10.1364/PRJ.7.000332

1. INTRODUCTION

Mode-locked fiber lasers, especially those passively mode locked by employing saturable absorbers, have attracted intensive investigation in recent years, mainly motivated by two aspects. One is that some novel materials exhibiting saturable absorption continuously emerged and gained extensive attention, such as graphene [1–5], topological insulators [6–8], black phosphorus [9–12], and MXene [13]. The other is attributed to the rich phenomena and dynamics relating to passive mode locking in fiber lasers, besides some typical solitons, that still deserve revelation or further investigating, such as bunched multiple solitons [7], vector solitons [11], bound-state solitons [12], soliton rains [14], soliton molecules [15], dark pulses [16], and dissipative soliton resonances [17,18].

Most investigations have been devoted to fundamental mode locking (FML), which produces a single pulse in one cavity roundtrip, resulting in a pulse repetition frequency (PRF) directly defined by the cavity length. FML represents the standard mode-locked operation of lasers that exhibits the highest stability. In addition to that, harmonic mode locking (HML) is a particular multiple-pulse phenomenon that exhibits equal pulse intervals among adjacent pulses, i.e., the multiple pulses occupy the cavity uniformly through self-rearrangement, resulting in a state of operation at a multiple of the cavity-length-determined fundamental PRF. It has been considered an attractive route to enhance the PRF of a passively mode-locked fiber laser in an integral multiple manner, through intense pumping and appropriate setting of the cavity-related parameters.

HML has been achieved in various mode-locking regimes, such as solitons [19–22], bound-state solitons [23], twin-pulse solitons [24], soliton bunches [25], dissipative solitons [26,27], dissipative soliton resonances (DSRs) [28,29], and dark pulses [30–32]. Relying on wave-breaking-free properties attributed to the peak-power-clamping (PPC) effect, DSR has recently been shown to be a promising mode-locking regime that could scale the pulse energy to virtually unlimited levels, and, in fact,

up to 10 μJ single pulse energy from a fiber laser oscillator was achieved by Semaan *et al.* [33]. The detailed amplifying characteristics of DSR pulses at the 2 μm band were investigated by Zhao *et al.*, and over 94 μJ amplified pulse energy was obtained with up to ~18.4 kW peak power from a thulium-doped fiber (TDF) master oscillator power amplifier (MOPA) system [34]. However, despite the unparalleled scalability in single pulse energy, HML was still observed in the DSR regime [28,29,35]. It is suspected that the initial condition causes the HML [36], or the pulse energy limiting effect might be induced with some specific settings in the cavity, such as the polarization state (PS) or the spectral-filtering effect.

The most intensively investigated DSR pulses exhibit a well-known square wave or rectangular shape. DSR pulses can form in both normal and anomalous dispersion regimes. However, due to soliton effects (pulse energy limiting, soliton splitting, etc.) some noise-like square wave pulses can also be easily produced from a fiber oscillator. Even if sharing a similar pulse shape, the noise-like square wave pulses are quite different from typical DSR pulses. Although a noise-like square wave pulse looks like a single pulse from an oscilloscope with a slow responding photodetector, a measurement by using an autocorrelator showed that it contained some fine structures on the square long envelope [37].

In addition to the DSR pulse exhibiting a square wave envelope, some other related pulse envelopes have also been observed, such as that with a tilt-top [38,39]. For some other particular pulses, although they, strictly speaking, could not be identified as in the DSR regime, there were some similarities between them and the DSR pulse in an envelope, such as chair-like pulses [40] and step-like pulses [41]. Very recently, we observed another particular type of h-shaped pulse [42]. It had a narrow leading edge, similar to a sharp peak, and, meanwhile, showed some similar behaviors on its trailing portion with the DSR pulse, mainly including the well-known PPC effect and pump-power-dependent duration. As what has just been confirmed by Luo *et al.* most recently [43], this type of pulse also shared some of the advantages of the DSR pulse that were favorable by gain switching, such as long-enough pump-dependent pulse duration, freedom from wave breaking, and high pulse energy. They achieved ~0.79 μJ of pulse energy at 2.103 μm with a repetition rate of 1.435 MHz from a holmium-doped fiber laser gain switched by a TDF MOPA seeded with an h-shaped pulse source that they built. The built fiber laser cavity was ~137.2 m long, and the achieved pulse duration was several nanoseconds.

Although some single h-shaped pulse characteristics have been investigated experimentally in TDF lasers, there is still no investigation of the related HML. There should be some possibility that an HML state of the h-shaped pulses might exist under some specific cavity designs and operation conditions, considering the observed similarities between the h-shaped and DSR pulses. In this paper, we demonstrated that tunable and switchable HML of h-shaped pulses could indeed be achieved if the cavity length was long enough, with some controllable conditions. In detail, we built a TDF laser resonator reaching ~3.03 km with an ultralarge anomalous dispersion over −200 ps^2 around the emission wavelength, which is the longest cavity and the largest dispersion for a TDF laser ever built, to the best of our knowledge. We also further investigated the related evolution and switching characteristics with respect to the pump power and PS, respectively.

2. EXPERIMENTAL SETUP

Figure 1 schematically shows the employed experimental layout. The fiber laser resonator was constructed with a typical figure-eight (f-8) configuration. The pump source was a compact all-fiber MOPA system including a single-frequency wavelength-tunable distributed-feedback laser diode (DFB-LD) and an erbium-ytterbium fiber amplifier (EYFA). To enhance pump absorption, the emission wavelength of the MOPA system should be as long as possible toward the peak absorption of the TDF in the 1.6–1.7 μm region. For that, the peak wavelength of the seeding DFB-LD was tuned to its long-wavelength limit of ~1570.4 nm with ~5.3 mW continuous wave (CW) output power. The whole MOPA system could provide CW and nearly single-frequency output power continuously tunable from less than 100 mW to over 4 W at ~1570.4 nm.

Through a filter wavelength division multiplexer (FWDM), the pump light was coupled into a piece of TDF with a length of only ~16 cm. The TDF exhibits a specified core absorption of ~500 dB/m at 793 nm, core numerical aperture (NA) of 0.15, and core/cladding diameters of 10/130 μm, respectively. We used the 82% port of an 18/82 fiber optical coupler (FOC) as the output for achieving high enough output power. To enable unidirectional propagation of the produced signal laser in the gain fiber, an isolator was used at the other side of the FWDM. Through a 20/80 FOC, an asymmetric nonlinear optical loop mirror (NOLM) was constructed, in which a fiber spool with ~3.021 km long SMF-28e fiber was incorporated to lengthen the cavity and enhance the cumulative nonlinearity. Without any isolation, the split laser beams propagated bidirectionally in the NOLM, and then underwent interference at the FOC. Two manual fiber polarization controllers (FPCs), one being the three-paddle type and the other the in-line type, were incorporated into the fiber laser resonator to manipulate the intra-cavity PS. For the three-paddle FPC used in the gain fiber loop, i.e., FPC-1, its three paddles consist of four, eight, and four loops of SMF-28e in series, with the same loop diameter of ~56 mm. Correspondingly, they roughly create a quarter-wave plate, a half-wave plate, and a quarter-wave plate, respectively. For the in-line FPC incorporated in the NOLM, i.e., FPC-2, the induced retardance can be tuned by adjusting the pressure and rotating the fiber squeezer.

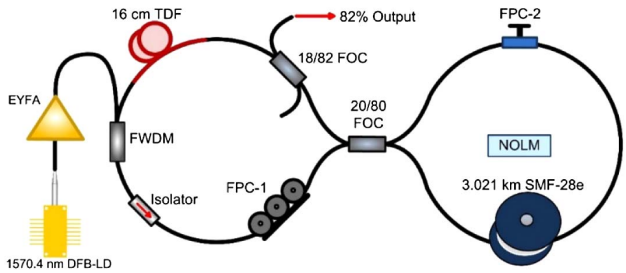

Fig. 1. Experimental layout.

The total geometrical length of the constructed fiber laser cavity was ~3.03 km. Apart from the ~16 cm TDF, all fiber pieces used were Corning SMF-28e, which has a large value of anomalous dispersion around the 2 μm band. This resulted in an ultralarge anomalous dispersion over −200 ps^2 estimated at the emission wavelength.

3. RESULTS AND DISCUSSION

When the pump power increased to ~1.46 W, CW lasing started. The pumping threshold is ~1.58 W for stable FML operation that could deliver a single h-shaped pulse when the two FPCs were adjusted to appropriate orientations. Because of the ultralarge length of the fiber laser resonator, the generated pulse train exhibited an ultralong repetition period of ~14.88 μs, which was also the cavity roundtrip time and corresponded to an ultralow PRF of ~67.22 kHz. This indicates that FML with single h-shaped pulse emission was still possible even when the laser cavity reached several kilometers long. HML emission could be observed with further increasing pump power above a threshold value, when orientations of the two FPCs were fixed, i.e., the intra-cavity PS was locked to a particular one. We further observed that both the pump power and intra-cavity PS could considerably affect the characteristics of the h-shaped pulse trains as well as each individual pulse. Below, we will discuss these output characteristics in detail.

A. Pump-Power-Related Switching and Evolution

Figure 2 shows the detailed switching characteristics from the FML to some higher orders of HML with the pump power increasing. On the left, Figs. 2(a)–2(e) show several captured temporal traces with the same span, covering two repetition periods, i.e., two cavity roundtrips. It can be seen that all the temporal traces, no matter what the FML or the different orders of HML, contained pulses with distinctly h-shaped envelopes. With ~4.15 W pump power, the maximum pump power we utilized here, and the same fixed PS, up to 8th order of HML could be achieved, as seen from the pulse train shown in Fig. 2(e). It should be noted that all these pulse trains were recorded under identical conditions. All the temporal characteristics throughout this paper were measured by using a 2 μm InGaAs photodetector (PD, ET-5000, Electro-Optics Technology, Inc.) in combination with a real-time digital storage oscilloscope (DSO, DSO9104A, Agilent Technologies, Inc.). As specified, the PD has a bandwidth (BW) of >12.5 GHz and rise/fall time of 28 ps. The DSO exhibits a maximum sampling rate of 20 GSa/s, a typical rise/fall time of 253 ps (10%–90%), and a BW of 1 GHz. Considering the large recording temporal length along with too much time required, here we used a sampling rate of 5 GSa/s to record the pulse trains, rather than the maximum value.

Figures 2(f)–2(j) show several captured radio frequency (RF) traces corresponding to the left side temporal traces, which were directly detected by using the same photodetector, but were further recorded by using an RF spectrum analyzer (N9320B, Agilent Technologies, Inc.). Here, the recording span was 10 MHz with a resolution BW (RBW) of 100 Hz. For each trace, despite the comb-like frequency lines determined by the PRF, the large-scale modulation pattern across them resulted from the long temporal duration of the lower part of each h-shaped pulse. Mathematically, the modulation frequency and that temporal duration satisfied a reciprocal relationship.

Figure 3 plots the spectral profiles corresponding to the h-shaped pulses shown in Fig. 2, measured by using a long wavelength optical spectrum analyzer (OSA, AQ6375B, Yokogawa Test & Measurement Co.) with a setting resolution of 0.05 nm. As can be seen, the highly structured spectral profiles, particularly the pronounced sharp cuts distributed across them, were mainly caused by the absorption lines of atmospheric molecules, primarily of water [44]. Despite the structured profiles, we could still roughly discern the spectral evolution with pump power. First, the higher the pump power, the broader the spectra spanned. Second, there was a minor redshift on the peak wavelength, i.e., ~1846.42–~1850.18 nm as the pump power increased from ~1.58 to ~4.15 W.

In a fixed PS and before the laser switched from one state to another, temporal characteristics of the output pulse could be continuously varied with the pump power. Figure 4 plots several pulse envelopes with different pump powers when

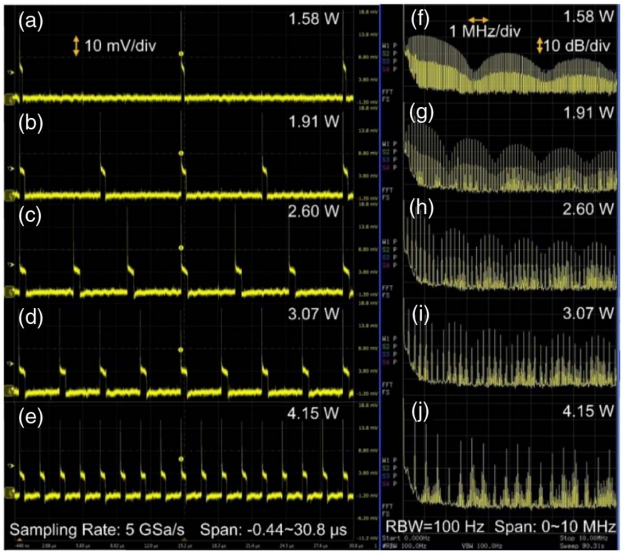

Fig. 2. Pump power induced harmonic switching with the (a)–(e) pulse trains and (f)–(j) RF spectra.

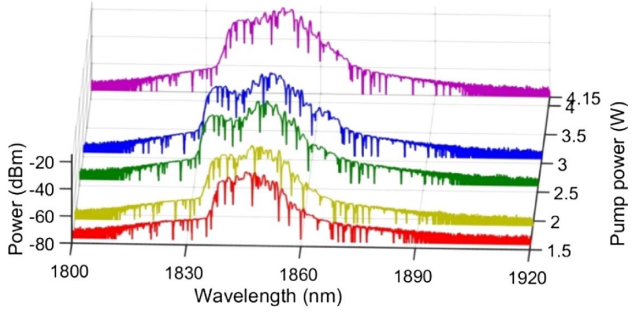

Fig. 3. Output optical spectra with different pump powers, also corresponding to different orders of HML.

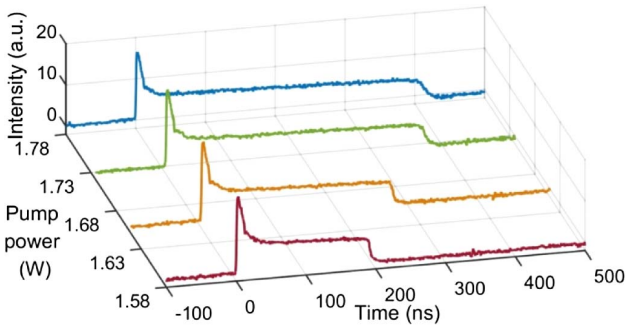

Fig. 4. Pump-power-induced evolution with the single pulse envelope when the TDF laser is operated with a fundamental repetition rate.

the TDF laser operated with FML. The lower part of the pulse duration, estimated at half the amplitude of the trailing edge, extended from ~180 to ~410 ns as the pump power increased from ~1.58 to ~1.78 W, which was similar to the temporal characteristics of fiber lasers working in a typical DSR regime [17,18]. As could be seen, each pulse exhibited a sharp leading peak and a following flat trailing portion, more clearly showing an h-like shape. Another noticeable characteristic was that the trailing portion remained roughly unchanged with the pump power. This was also quite similar to the case of the DSR regime. These temporal characteristics of the flat trailing portion were just due to the PPC effect.

In addition, it should be noted that the trailing portion did not result from amplified spontaneous emission (ASE), although some similarities might be shared. In a fiber amplifier with ultralow repetitive seeding pulses (typically less than tens of kilohertz), ASE can arise if the pump is continuous. In our fiber laser, however, the PRF was high enough, particularly with the HML, with which it was not so easy to induce significant ASE in the pulse intervals. Moreover, compared to the single-pass fiber amplifier, the oscillating characteristics of the fiber laser could also provide some suppression on the ASE.

These evolution characteristics are consistent with our previous observations in Ref. [42], but no HML was observed there. These observations indicate that the h-shaped pulse formation partially results from the PPC effect. This effect flattens the long trailing portion and prevents pulse splitting, no matter whether it is with the FML or HML state. However, we are so far not sure how the sharp leading part of the h-shaped pulse is generated. The HML of the h-shaped pulses, as a particular multiple pulse phenomenon, is due to a pump power that is too strong and to limited pulse energy. Then, due to the self-rearrangement process in the fiber laser, the multiple pulses can occupy the cavity in a uniform manner, finally resulting in HML formation.

B. PS-Induced Switching Characteristics

In addition to the pump power related evolution and switching characteristics of the h-shaped pulses in FML and HML, another interesting issue is whether the PS can affect the operating state of the TDF laser. To confirm it, we then conducted an experiment in which the intra-cavity PS was manipulated through adjusting the two FPCs while the output characteristics were monitored simultaneously. It was then verified that, although our cavity length reached several kilometers, the achievable pulse energy was still highly influenced by the intra-cavity PS, which resulted in the PS dependences of the HML.

The HML could be switched from 8th up to 48th order by simply manipulating the PS when the pump power was fixed at ~4.15 W. Figure 5 shows several captured pulse trains for some of those different orders of HML. It can be seen that, as the HML switches from a lower to a higher order, the peak intensity lowers rapidly, and the duration of the trailing portion narrowed down, from ~491 to ~85 ns. However, no significant change in the intensity of the trailing portion could be observed.

The 48th order of HML is the highest one we can achieve presently. Although much higher orders of HML have been observed and reported in other ultrashort soliton mode-locking regimes [45,46], HML of h-shaped pulses with high order would encounter one intrinsic problem. As we know, ultrashort soliton operations typically exhibit an extremely large pulse interval in contrast to its ultrashort pulse duration, which results in a tiny pulse duty circle (PDC). Because of the basic limitation in soliton energy according to the well-known area theorem, a soliton very readily splits under intensive pumping, particularly in an ultralong cavity and all-anomalous-dispersion regime. That is why soliton operation can easily reach a high

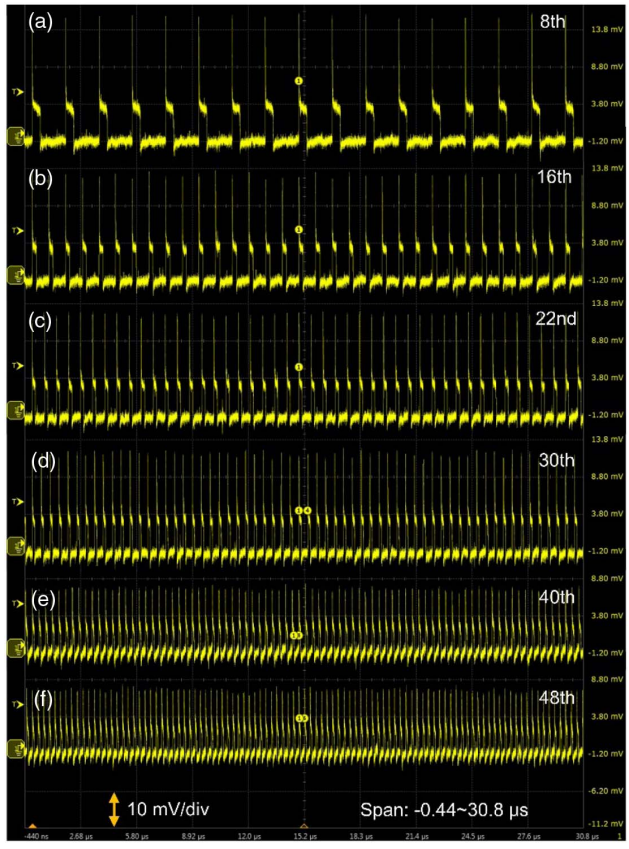

Fig. 5. Several pulse trains with different orders of HML switched by PS manipulation with a fixed pump power of ~4.15 W.

order of HML. For the h-shaped pulse, however, it typically has a long duration evaluated by considering the trailing portion if an ultralong cavity is employed and an intensive pump is applied. For our case, the achieved longest duration reached over 600 ns [Fig. 2(c)], which was 10^6 (one million) times longer than typical soliton pulses. This means that, for an identical condition, the h-shaped pulses could have a PDC several orders higher than that of typical solitons. Thus, for too high an order of HML, the long trailing portion of the h-shaped pulses would fully occupy the pulse intervals, i.e., adjacent pulses would nearly overlap with each other. In the experimental aspect, however, the pulses would typically merge into a CW operation rather than forming a pulse overlap state, like what we observed in our previous publication, where the PDC could approach 98.2% but its further increase would result in transformation into a CW state [34].

In addition to the intrinsic issue, other factors on the limitation of the highest order of HML, i.e., 48th order here, mainly included the available pump power, the large attenuation loss of silica fibers at the 2 μm band, and particularly the hindering of pulse splitting due to the PPC effect that we discussed at the end of Section 3.A. If we consider some other approaches like utilizing the acoustic stabilization effect adopted in Refs. [45,46], higher orders of pulses might be possible, but it cannot ensure that the laser would still be able to operate in the h-shaped pulse regime then.

We have also tried to measure the autocorrelation trace of the h-shaped pulse to confirm if there were some fine structures or noise-like tiny pulses hidden in the long pulse packet. No matter how we varied the pump power and manipulated the PS, there was no noticeable short trace that could be observed within the maximum span of our available autocorrelator (APE, Angewandte Physik & Elektronik GmbH, PulseCheck). We prefer that there are no fine structures or noise-like pulses hidden in the trailing portion of the h-shaped packet, although further experimental evidence is required for this claim.

Supermodes can typically be produced in an HML fiber laser [19]. In the HML operation of the h-shaped pulses, we also observed the supermodes along with the main PRF lines, as seen from the RF traces in Fig. 6, which were recorded with an RBW of 10 Hz and a span of 0–4 MHz. Only clean RF lines could be observed with the FML, as seen in Fig. 6(a). However, supermode lines appeared between the main PRF lines, once the laser switched to an HML state either by increasing the pump power or by manipulating the PS. The higher the order of HML, the stronger the generated supermodes, i.e., the lower the supermode suppression ratio (SMSR). Taking the 16th order of HML, for instance, as seen in Fig. 6(e), the SMSR was ~38.6 dB, whereas it decreased to ~12.8 dB when the HML reached 48th order [Fig. 6(h)].

In addition to PS-tuning effectively enabling the HML-order switching, it was noted that a specific FPC location could also exert some influence on the temporal characteristics. The switching characteristics relating to both the PS tuning and FPC location could be understood as follows.

In principle, adjusting the paddle(s) or fiber squeezer of an FPC will vary the local fiber birefringence, which results in a change on the induced phase retardance. For FPC-1, if it was placed prior to the TDF, the induced retardance experienced some amplification due to the fiber gain compared to where it was placed after the TDF, as in Fig. 1. However, no matter where it was placed, it seemed no significant difference on the transmittance of the NOLM was induced by its specific location because of the unidirectional propagation enabled by the isolator. Alternatively, rotating any paddle of FPC-1, in any case, could vary the output pulse characteristics considerably, which was probably due to the resulting change in the total cavity birefringence, similar to the case we observed in our previous publication [42]. In detail, although FPC-1 did not directly vary the transmittance of the NOLM, it could vary the overall cavity birefringence by inducing some additional amount of fiber birefringence. This further resulted in change in the PS of the input pulse to the NOLM, i.e., altering the coupling between the two orthogonal field components of the pulse. This induced a different nonlinear phase retardance $\Delta\phi_{\mathrm{NL}}$ within the NOLM, corresponding to a change of the transmittance of the NOLM. Thus, FPC-1 could vary the transmittance of the NOLM in an indirect manner, but somehow it could influence the output pulse characteristics considerably.

For FPC-2, however, we noticed that its specific location could indeed affect the output pulse characteristics. Most noticeably, placing FPC-2 near the 80% port of the FOC could vary the pulse characteristics much more dramatically than placing it near the 20% port, where we have assumed that the input was provided by the port connecting FPC-1. The probable reason might be understood from the resulting

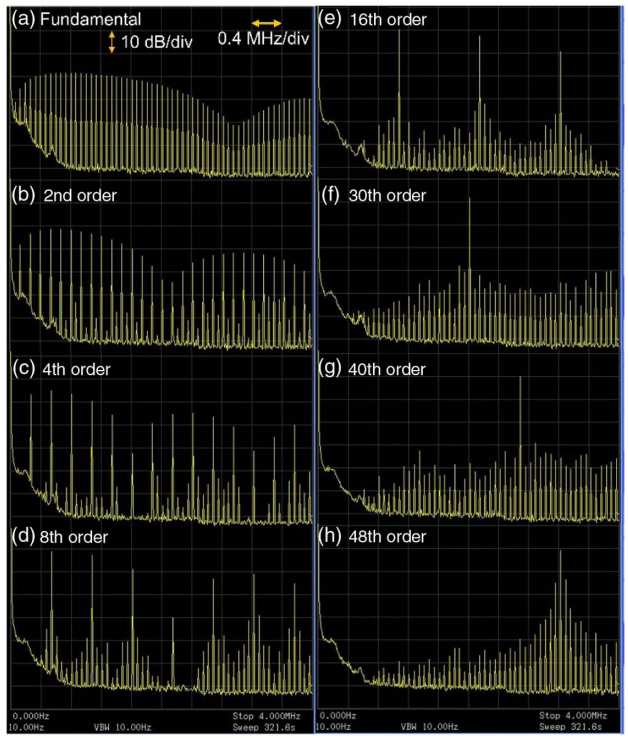

Fig. 6. Detailed RF characteristics with the (a) FML and (b)–(h) different orders of HML.

different transmittances of the NOLM with these two locations. The details can be analyzed as follows.

The pulse peak power from the 80% port is higher than that from the 20% port, which experiences a larger nonlinear phase shift ϕ_{NL} comparatively in the NOLM. ϕ_{NL} can be calculated by using the formula [47]

$$\phi_{NL} = \frac{2\pi n_2}{\lambda A_{eff}} P_0 L_{eff}. \quad (1)$$

Here, n_2 is the nonlinear-index coefficient, λ is the light wavelength in vacuum, A_{eff} is the effective mode area of the fiber (here SMF-28e), P_0 is the pulse peak power, and L_{eff} is the effective propagation. L_{eff} is approximately the length of the NOLM by neglecting its loss. Except for P_0, all other parameters in Eq. (1) can be considered constant values. Thus, if the peak power difference between the counterpropagating pulses in the NOLM is noted as ΔP, the resulting phase retardance $\Delta\phi_{NL}$ between the two beams, when they arrive at the FOC again after counterpropagating through the NOLM, is

$$\Delta\phi_{NL} = \frac{2\pi n_2 L_{eff}}{\lambda A_{eff}} \Delta P = (1-2\alpha)\frac{2\pi n_2 L_{eff}}{\lambda A_{eff}} P_{in}. \quad (2)$$

P_{in} is the input pulse peak power of the NOLM. In Eq. (2), we have related ΔP with P_{in} as $\Delta P = (1-2\alpha)P_{in}$, with α being the splitting ratio of the FOC (here $\alpha = 0.2$).

With no other retardance, the transmittance T of the NOLM will be determined solely by $\Delta\phi_{NL}$ as the following relationship [48]:

$$T = 1 - 2\alpha(1-\alpha)[1 + \cos(\Delta\phi_{NL})]. \quad (3)$$

However, if FPC-2 is tuned to produce an additional retardance, noted as $\Delta\phi_{FPC}$, T will be changed. Moreover, T is dependent on the location of the FPC in the NOLM and roughly satisfies

$$T = 1 - 2\alpha(1-\alpha)[1 + \cos(\Delta\phi_{NL} \pm \Delta\phi_{FPC})]. \quad (4)$$

If FPC-2 is placed near the 80% port of the FOC, a + sign should be chosen. Otherwise, a − sign should be chosen if it is placed near the 20% port. Further taking a derivative of T with respect to $(\Delta\phi_{NL} \pm \Delta\phi_{FPC})$, we obtain

$$\frac{dT}{d(\Delta\phi_{NL} \pm \Delta\phi_{FPC})} = 2\alpha(1-\alpha)\sin(\Delta\phi_{NL} \pm \Delta\phi_{FPC}). \quad (5)$$

For the FML, the pulse peak power is roughly 3 times the power of the flat trailing portion, as shown in Fig. 5(a), which can be roughly calculated as ~1.25 W. Based on Eq. (2), $\Delta\phi_{NL} \approx 4.003$ rad through calculation. By substituting this value into Eq. (5), it can be seen that, compared to the resulting value without $\Delta\phi_{FPC}$, a larger rate of change in T would be induced for a small positive value of $\Delta\phi_{FPC}$; conversely, a smaller one would be induced for a small but negative value of $\Delta\phi_{FPC}$. Thus, it would be easier to obtain a more dramatic change in the pulse characteristics if FPC-2 is placed near the 80% port comparatively. In fact, we have placed it there, as shown in Fig. 1, for achieving as many HML states as possible from the FML through tuning the FPC-2.

From Eqs. (4) and (5), no matter the location of FPC-2, i.e., no matter whether a + or − sign might be chosen, $\Delta\phi_{FPC}$ could induce some change in the transmittance of the NOLM, which could further vary the overall characteristics of the mode locking. Most significantly, this could induce HML order switching. Certainly, the FPC-2 might also be placed at other locations in the NOLM. According to Eqs. (4) and (5), some intermediate tuning effects might be achievable compared to the two extreme cases just discussed.

Despite the FPC-related switching characteristics of the HML, we further noticed that when the pump power was too high, it was impossible to obtain the FML, no matter how the two FPCs were adjusted. Taking the ~4.15 W pump power, for instance, the obtainable lowest order of HML was 8th. This indicated that the h-shaped pulse could not be a type of energy-unlimited pulse under some extreme conditions, like the ultra-large length of the cavity here. In a more in-depth way, with high-enough pump power, strong-enough nonlinearity, and large-enough dispersion, the prevention of the pulse-splitting effect of the h-shaped pulse became impossible through typical approaches, such as PS manipulation.

As a short summary, the switching of HML could be achieved by two methods: one is to simply vary the pump power with fixed PS; the other one is to change the PS with fixed pump power. The former one is achieved due to the limited PPC effect. Consequently, the varying pump power will change the pulse number. The latter is achieved by changing the supported pulse energy, hence, the pulse number changes as the total output power is nearly maintained.

C. Other HML-Order-Related Characteristics

To further understand the possible mechanisms behind the HML of h-shaped pulses, it should also be helpful to compare the detailed characteristics of each individual pulse with pump-power-related different orders of HML. We then plotted them as shown in Fig. 7. As can be seen, both the leading and trailing portions of each h-shaped pulse decrease as it splits into more pulses with higher orders of HML, which was achieved by increasing the pump power. This might indicate that it was the pulse splitting that altered the PPC effect, rather than that the latter induced the former. Thus, although the clamped peak powers exhibited some changes for different orders of HML, the PPC effect should still be able to shape the h-shaped pulses (at least on the trailing portions), both with the FML as we claimed in Ref. [42] and with the HML here. However, the PPC effect should not be the cause for HML. In fact, the PPC effect could somehow hinder the laser developing into a higher order HML by preventing pulse breaking or splitting.

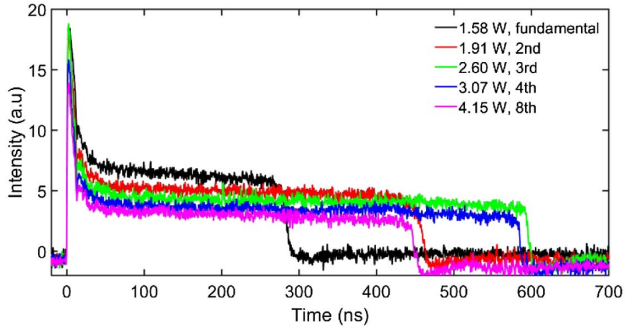

Fig. 7. Detailed pulse envelope of each individual h-shaped pulse with PS-fixed pump-power-related different orders of HML.

HML of the h-shaped pulse might be due to other factors, such as nonlinearity, birefringence, or spectral filtering, as well as other higher order (over the 2nd order) effects, although it is currently still beyond our ability to reach an exact conclusion on which one or even which combination of several of them dominated this phenomenon. These factors caused some limitation on the PPC effect, which further resulted in pulse breaking, i.e., the laser being switched to a higher order of HML.

From Fig. 7, it could also be noticed that the duration of the flat trailing portion was not linear or at least not monotonic with the pump power, which was caused by the switching among different orders of HML. The details are as follows. It was found that, only with the same order of HML or with the FML, the pulse peak power could be clamped to a certain value, and the duration of the pulse trailing portion would increase almost linearly with the pump power. After being switched to a different order of HML, however, the pulse duration would experience a sudden change due to the pulse splitting or merging, and then the new pulse envelope would follow a linear evolution again with the pump power, until next switching to a different HML order. Because both the trailing duration immediately after a splitting or merging and the further broadening in duration due to the PPC effect might be different, the recorded trailing duration did not follow a monotonic evolution with respect to the HML order.

Another interesting issue was how the pulse peak duration might vary with the pump power and HML order. Although the responses of both the available photodetector and oscilloscope were limited, they should be able to give some rough measurements considering that the pulse peak durations were in the nanosecond range (as previously mentioned, the autocorrelation measurement cannot be used to confirm if there were some ultrashort fine structures embedded). The measured results are shown in Fig. 8.

As illustrated in the inset of Fig. 8(a), the pulse peak duration was evaluated at the points on the pulse envelope where the power $P_{1/2,\mathrm{peak}}$ related to the sharp peak leading power P_{leading} and the trailing portion power P_{trailing} as

$$P_{1/2,\mathrm{peak}} = P_{\mathrm{trailing}} + \frac{1}{2}(P_{\mathrm{leading}} - P_{\mathrm{trailing}}) = \frac{1}{2}(P_{\mathrm{leading}} + P_{\mathrm{trailing}}). \quad (6)$$

Figure 8(a) plots its evolution with the pump power. As can be seen, it narrowed as the pump power increased with the FML, although the trailing portion broadened in this process, as seen in Fig. 4. As also noticed, narrowing also occurred with the pulse switching to some higher order of HML. Much differently than with PS tuning, however, the pulse peak duration increased with the HML switching into a higher order when the pump power was fixed to ~4.15 W, as seen in Fig. 8(b). The difference might be understood by comparing Figs. 2 and 5. In Fig. 2, it could be noticed that, although the laser transformed to some higher orders of HML as the pump power increased above the related threshold values, no such lowering in the pulse peak power could be observed. Thus, it could be intuitively deduced that the pulse duration narrowing was possible considering the process with a pulse abruptly breaking into more pulses with similar peak powers. From Fig. 5, however, much more significant lowering in pulse peak power could be observed. Thus, the evaluation points on the pulse peak duration would be much closer to the trailing portion, i.e., $P_{1/2,\mathrm{peak}} \to P_{\mathrm{trailing}}$, which would make the evaluated peak duration longer. This might be why we observed the peak duration increasing with the HML-order, in Fig. 8(b), when we tuned the two FPCs without varying the pump power.

Although the plots showed some differences in Figs. 8(a) and 8(b), they all followed some monotonic trends, which were quite different from the characteristics of the trailing portion shown in Fig. 7. This further indicated that the peak leading portion might be at least incompletely clamped, and the PPC effect was quite weak or even negligible in shaping the sharp peak. Thus, this portion should follow evolutions similar to other typical pulses without the PPC effect.

For the PS-related different orders of HML, the emitted average output power also showed some PS dependences. As the plots in Fig. 9 show, all the power evolutions under different PSs showed roughly linear tendencies with pump power. Moreover, from the calculated slope efficiencies, it could be seen that the higher the achieved order of HML, the higher the corresponding slope efficiency, i.e., the larger average output power. This indicated that a higher order of HML should be preferably achieved with a higher effective laser gain, and the

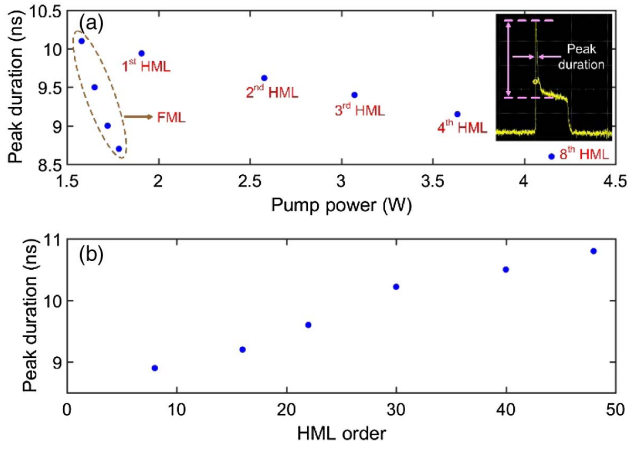

Fig. 8. Evolutions of pulse peak duration with respect to the (a) pump power with a fixed PS, and (b) HML order with a fixed pump power.

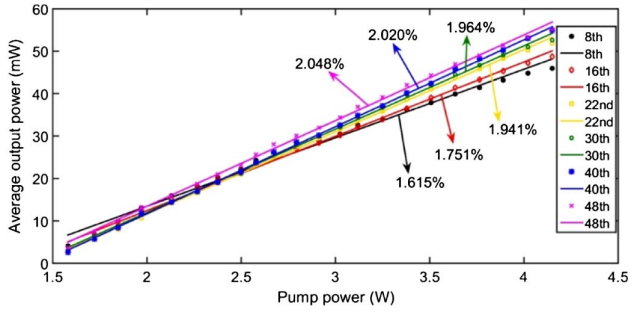

Fig. 9. Average output power versus pump power for PS-induced different orders of HML.

effective laser gain should be partially determined by the intra-cavity PS.

4. CONCLUSION

In conclusion, we have experimentally investigated the HML characteristics of a type of h-shaped pulses produced in an NOLM-mode-locked TDF laser with ultralong cavity and ultralarge anomalous dispersion. Both the pump power and PS-related evolution and switching behaviors were observed in the HML. For each individual pulse, pump-power-induced broadening occurred no matter with the FML or with some higher order of HML. Further discussions and analyses were also given on the related mechanisms with those experimental observations. Our results experimentally verified that a single h-shaped pulse can exist even in a kilometers-long fiber laser resonator, and its HML could be achieved and switched through appropriate manipulations of the pump power and intra-cavity PS.

Funding. Natural Science Foundation of Jiangsu Province, China (BK20170243); National Natural Science Foundation of China (NSFC) (61705094, 11674133, 11711530208, 61575089); Key Research Program of Natural Science of Jiangsu Higher Education Institutions (17KJA416004); Royal Society (IE161214); Protocol of the 37th Session of China-Poland Scientific and Technological Cooperation Committee (37-17); H2020 Marie Skłodowska-Curie Actions (MSCA) (790666); Jiangsu Overseas Visiting Scholar Program for University Prominent Young and Middle-aged Teachers and Presidents; Priority Academic Program Development of Jiangsu Higher Education Institutions (PAPD).

REFERENCES

1. Q. Bao, H. Zhang, Y. Wang, Z. Ni, Y. Yan, Z. X. Shen, K. P. Loh, and D. Y. Tang, "Atomic-layer graphene as a saturable absorber for ultrafast pulsed lasers," Adv. Funct. Mater. **19**, 3077–3083 (2009).
2. H. Zhang, Q. Bao, D. Tang, L. Zhao, and K. Loh, "Large energy soliton erbium-doped fiber laser with a graphene-polymer composite mode locker," Appl. Phys. Lett. **95**, 141103 (2009).
3. H. Zhang, D. Y. Tang, L. M. Zhao, Q. L. Bao, and K. P. Loh, "Large energy mode locking of an erbium-doped fiber laser with atomic layer graphene," Opt. Express **17**, 17630–17635 (2009).
4. Z. Sun, T. Hasan, F. Torrisi, D. Popa, G. Privitera, F. Wang, F. Bonaccorso, D. M. Basko, and A. C. Ferrari, "Graphene mode-locked ultrafast laser," ACS Nano **4**, 803–810 (2010).
5. Z. Sun, D. Popa, T. Hasan, F. Torrisi, F. Wang, E. J. R. Kelleher, J. C. Travers, V. Nicolosi, and A. C. Ferrari, "A stable, wideband tunable, near transform-limited, graphene-mode-locked, ultrafast laser," Nano Res. **3**, 653–660 (2010).
6. C. Zhao, Y. Zou, Y. Chen, Z. Wang, S. Lu, H. Zhang, S. Wen, and D. Tang, "Wavelength-tunable picosecond soliton fiber laser with topological insulator: Bi_2Se_3 as a mode locker," Opt. Express **20**, 27888–27895 (2012).
7. Y. Chen, M. Wu, P. Tang, S. Chen, J. Du, G. Jiang, Y. Li, C. Zhao, H. Zhang, and S. Wen, "The formation of various multi-soliton patterns and noise-like pulse in a fiber laser passively mode-locked by a topological insulator based saturable absorber," Laser Phys. Lett. **11**, 055101 (2014).
8. P. Yan, R. Lin, H. Chen, H. Zhang, A. Liu, H. Yang, and S. Ruan, "Topological insulator solution filled in photonic crystal fiber for passive mode-locked fiber laser," IEEE Photon. Technol. Lett. **27**, 264–267 (2015).
9. Y. Chen, G. Jiang, S. Chen, Z. Guo, X. Yu, C. Zhao, H. Zhang, Q. Bao, S. Wen, D. Tang, and D. Fan, "Mechanically exfoliated black phosphorus as a new saturable absorber for both *Q*-switching and mode-locking laser operation," Opt. Express **23**, 12823–12833 (2015).
10. Z. Luo, M. Liu, Z. Guo, X. Jiang, A. Luo, C. Zhao, X. Yu, W. Xu, and H. Zhang, "Microfiber-based few-layer black phosphorus saturable absorber for ultra-fast fiber laser," Opt. Express **23**, 20030–20039 (2015).
11. Y. Song, S. Chen, Q. Zhang, L. Li, L. Zhao, H. Zhang, and D. Tang, "Vector soliton fiber laser passively mode locked by few layer black phosphorus-based optical saturable absorber," Opt. Express **24**, 25933–25942 (2016).
12. Z. Wang, Y. Xu, S. C. Dhanabalan, J. Sophia, C. Zhao, C. Xu, Y. Xiang, J. Li, and H. Zhang, "Black phosphorus quantum dots as an efficient saturable absorber for bound soliton operation in an erbium doped fiber laser," IEEE Photon. J. **8**, 1503310 (2016).
13. X. Jiang, S. Liu, W. Liang, S. Luo, Z. He, Y. Ge, H. Wang, R. Cao, F. Zhang, Q. Wen, J. Li, Q. Bao, D. Fan, and H. Zhang, "Broadband nonlinear photonics in few-layer MXene $Ti_3C_2T_x$ (T = F, O, or OH)," Laser Photon. Rev. **12**, 1700229 (2018).
14. S. Chouli and P. Grelu, "Rains of solitons in a fiber laser," Opt. Express **17**, 11776–11781 (2009).
15. X. Liu, X. Yao, and Y. Cui, "Real-time observation of the buildup of soliton molecules," Phys. Rev. Lett. **121**, 023905 (2018).
16. H. Zhang, D. Y. Tang, L. M. Zhao, and X. Wu, "Dark pulse emission of a fiber laser," Phys. Rev. A **80**, 045803 (2009).
17. W. Chang, A. Ankiewicz, J. M. Soto-Crespo, and N. Akhmediev, "Dissipative soliton resonances," Phys. Rev. A **78**, 023830 (2008).
18. X. Wu, D. Y. Tang, H. Zhang, and L. M. Zhao, "Dissipative soliton resonance in an all-normal-dispersion erbium-doped fiber laser," Opt. Express **17**, 5580–5584 (2009).
19. C. Mou, R. Arif, A. Rozhin, and S. Turitsyn, "Passively harmonic mode locked erbium doped fiber soliton laser with carbon nanotubes based saturable absorber," Opt. Mater. Express **2**, 884–890 (2012).
20. J. Du, S. M. Zhang, H. F. Li, Y. C. Meng, X. L. Li, and Y. P. Hao, "L-band passively harmonic mode-locked fiber laser based on a graphene saturable absorber," Laser Phys. Lett. **9**, 896–900 (2012).
21. Z. Luo, M. Liu, H. Liu, X. Zheng, A. Luo, C. Zhao, H. Zhang, S. Wen, and W. Xu, "2 GHz passively harmonic mode-locked fiber laser by a microfiber-based topological insulator saturable absorber," Opt. Lett. **38**, 5212–5215 (2013).
22. M. Liu, A. Luo, W. Xu, and Z. Luo, "Coexistence of bound soliton and harmonic mode-locking soliton in an ultrafast fiber laser based on MoS_2-deposited microfiber photonic device," Chin. Opt. Lett. **16**, 020008 (2018).
23. Y. Wang, D. Mao, X. Gan, L. Han, C. Ma, T. Xi, Y. Zhang, W. Shang, S. Hua, and J. Zhao, "Harmonic mode locking of bound-state solitons fiber laser based on MoS_2 saturable absorber," Opt. Express **23**, 205–210 (2015).
24. B. Zhao, D. Y. Tang, P. Shum, W. S. Man, H. Y. Tam, Y. D. Gong, and C. Lu, "Passive harmonic mode locking of twin-pulse solitons in an erbium-doped fiber ring laser," Opt. Commun. **229**, 363–370 (2004).
25. L. M. Zhao, D. Y. Tang, T. H. Cheng, C. Lu, H. Y. Tam, X. Q. Fu, and S. C. Wen, "Passive harmonic mode locking of soliton bunches in a fiber ring laser," Opt. Quantum Electron. **40**, 1053–1064 (2008).
26. L. M. Zhao, D. Y. Tang, T. H. Cheng, H. Y. Tam, and C. Lu, "Passive harmonic mode locking of gain-guided solitons in erbium-doped fiber lasers," Chin. Sci. Bull. **53**, 676–680 (2008).
27. J. Peng, L. Zhan, S. Luo, and Q. Shen, "Passive harmonic mode-locking of dissipative solitons in a normal-dispersion Er-doped fiber laser," J. Lightwave Technol. **31**, 2709–2714 (2013).
28. Y. Lyu, H. Shi, C. Wei, H. Li, J. Li, and Y. Liu, "Harmonic dissipative soliton resonance pulses in a fiber ring laser at different values of anomalous dispersion," Photon. Res. **5**, 612–616 (2017).
29. G. Semaan, A. Niang, M. Salhi, and F. Sanchez, "Harmonic dissipative soliton resonance square pulses in an anomalous dispersion passively mode-locked fiber ring laser," Laser Phys. Lett. **14**, 055401 (2017).
30. X. Li, S. Zhang, Y. Meng, and Y. Hao, "Harmonic mode locking counterparts of dark pulse and dark-bright pulse pairs," Opt. Express **21**, 8409–8416 (2013).

31. J. Q. Zhao, Y. G. Wang, P. G. Yan, S. C. Ruan, G. L. Zhang, H. Q. Li, and Y. H. Tsang, "An L-band graphene-oxide mode-locked fiber laser delivering bright and dark pulses," Laser Phys. **23**, 075105 (2013).
32. R. Lin, Y. Wang, P. Yan, G. Zhang, J. Zhao, H. Li, S. Huang, G. Cao, and J. Duan, "Bright and dark square pulses generated from a graphene-oxide mode-locked ytterbium-doped fiber laser," IEEE Photon. J. **6**, 1500908 (2014).
33. G. Semaan, F. B. Braham, J. Fourmont, M. Salhi, F. Bahloul, and F. Sanchez, "10 μJ dissipative soliton resonance square pulse in a dual amplifier figure-of-eight double-clad Er:Yb mode-locked fiber laser," Opt. Lett. **41**, 4767–4770 (2016).
34. J. Zhao, D. Ouyang, Z. Zheng, M. Liu, X. Ren, C. Li, S. Ruan, and W. Xie, "100 W dissipative soliton resonances from a thulium-doped double-clad all-fiber-format MOPA system," Opt. Express **24**, 12072–12081 (2016).
35. C. Shang, X. Li, Z. Yang, S. Zhang, M. Han, and J. Liu, "Harmonic dissipative soliton resonance in an Yb-doped fiber laser," J. Lightwave Technol. **36**, 4932–4935 (2018).
36. A. Komarov, F. Amrani, A. Dmitriev, K. Komarov, and F. Sanchez, "Competition and coexistence of ultrashort pulses in passive mode-locked lasers under dissipative-soliton-resonance conditions," Phys. Rev. A **87**, 023838 (2013).
37. J. Liu, Y. Chen, P. Tang, C. Xu, C. Zhao, H. Zhang, and S. Wen, "Generation and evolution of mode-locked noise-like square-wave pulses in a large-anomalous-dispersion Er-doped ring fiber laser," Opt. Express **23**, 6418–6427 (2015).
38. J. Zhao, L. Li, L. Zhao, D. Tang, and D. Shen, "Dissipative soliton resonances in a mode-locked holmium-doped fiber laser," IEEE Photon. Technol. Lett. **30**, 1699–1702 (2018).
39. L. Zhao, D. Li, L. Li, X. Wang, Y. Geng, D. Shen, and L. Su, "Route to larger pulse energy in ultrafast fiber lasers," IEEE J. Sel. Top. Quantum Electron. **24**, 8800409 (2018).
40. P. K. Gupta, C. P. Singh, A. Singh, S. K. Sharma, P. K. Mukhopadhyay, and K. S. Bindra, "Chair-like pulses in an all-normal dispersion ytterbium-doped mode-locked fiber laser," Appl. Opt. **55**, 9961–9967 (2016).
41. D. Mao, X. Liu, L. Wang, H. Lu, and L. Duan, "Dual-wavelength step-like pulses in an ultra-large negative-dispersion fiber laser," Opt. Express **19**, 3996–4001 (2011).
42. J. Zhao, L. Li, L. Zhao, D. Tang, and D. Shen, "Cavity-birefringence-dependent h-shaped pulse generation in a thulium-holmium-doped fiber laser," Opt. Lett. **43**, 247–250 (2018).
43. H. Luo, F. Liu, J. Li, and Y. Liu, "High repetition rate gain-switched Ho-doped fiber laser at 2.103 μm pumped by h-shaped mode-locked Tm-doped fiber laser at 1.985 μm," Opt. Express **26**, 26485–26494 (2018).
44. F. Haxsen, D. Wandt, U. Morgner, J. Neumann, and D. Kracht, "Monotonically chirped pulse evolution in an ultrashort pulse thulium-doped fiber laser," Opt. Lett. **37**, 1014–1016 (2012).
45. M. S. Kang, N. Y. Joly, and P. St.J. Russell, "Passive mode-locking of fiber ring laser at the 337th harmonic using gigahertz acoustic core resonances," Opt. Lett. **38**, 561–563 (2013).
46. Q. Kuang, L. Zhan, Z. Wang, and M. Huang, "Up to the 1552nd order passively harmonic mode-locked Raman fiber laser," IEEE Photon. Technol. Lett. **27**, 2205–2208 (2015).
47. G. P. Agrawal, *Nonlinear Fiber Optics*, 5th ed. (Elsevier, 2013).
48. N. J. Doran and D. Wood, "Nonlinear-optical loop mirror," Opt. Lett. **13**, 56–58 (1988).